Muscle-Effort-Minimization-Inspired Kinematic Redundancy Resolution for Replicating Natural Posture of Human Arm

Quanlin Li, Yang Xia, Xianzong Wang, Peiyang Xin, Wenbin Chen, *Member, IEEE*, and Caihua Xiong, *Member, IEEE*

***Abstract*— Replicating natural postures of human arms is essential to generate human-like behaviors in robotic applications for humans nearby. However, how to realize this requirement in interactive scenarios remains a challenge due to the kinematic redundancy and unknown postural control strategy of human arms. Inspired by the physiological characteristics that the musculoskeletal system is coordinated to minimize muscle effort in human behaviors, this paper aims to address the issue by solving a muscle effort minimization problem. It adopts a high-fidelity human arm musculoskeletal model (HAMM) and considers the implicit constraint (desired hand pose) and the inequality constraints (range of joint motion). The constrained minimization is in general nonconvex, consequently sensitive to initial guesses in iterative procedures. So, it is impracticable to solve it directly with existing gradient-based deterministic approaches or standard evolutionary algorithms. As the main contribution, a hybrid inverse kinematics algorithm was proposed for the HAMM with 7 independent and 13 mimic joints to obtain the feasible arm postures satisfying the minimization constraints. Using the arm swivel angle that parametrizes the kinematic redundancy of the HAMM, geometrically equidistant initial guess candidates can be generated over the 1-dimension feasible posture manifold. As another contribution, we present a two-phase global minimization algorithm to handle the nonconvexity of the constrained minimization. It consists of a local-search phase on the null-space of the geometric Jacobian matrix and a global-search phase with an initial guess resampling strategy. The proposed approach was validated by replicating the natural arm postures of 5 right-handed subjects in daily tasks.**

***Index Terms*— Natural human arm posture, kinematic redundancy, musculoskeletal model, muscle effort, inverse kinematics.**

Manuscript received 24 November 2021; revised 26 June 2022; accepted 31 July 2022. Date of publication 11 August 2022; date of current version 26 August 2022. This work was supported in part by the National Key Research and Development Program under Grant 2018YFB1307201; and in part by the National Natural Science Foundation of China under Grant 52027806, Grant U1913601, Grant U1913205, and Grant 52075191. *(Corresponding authors: Caihua Xiong; Wenbin Chen.)*

This work involved human subjects or animals in its research. Approval of all ethical and experimental procedures and protocols was granted by the Clinical Trials Ethics Committee of Huazhong University of Science and Technology under Application No. IRB [2018]-235.

The authors are with the State Key Laboratory of Digital Manufacturing Equipment and Technology, Institute of Rehabilitation and Medical Robotics, Huazhong University of Science and Technology, Wuhan 430074, China (e-mail: chxiong@hust.edu.cn; wbchen@hust.edu.cn).

Digital Object Identifier 10.1109/TNSRE.2022.3198400

I. Introduction

As HUMAN-ROBOT collaboration gets closer and closer, robots must be human-aware [1]. Therefore, human-like motion capability is an essential requirement in robot applications for humans nearby due to social (e.g., robot likeability) and safety reasons (e.g., safety in human-robot interactions) [2]. This is helpful for humans to interpret and predict the motions of robots. Till now, significant progress has been made in mechatronic designs to implement human-like structures for robotic am-hand systems [3], [4], [5]. However, it remains a challenge to generate human-like behaviors for a human-like robotic arm-hand in case an accurate human demonstration is expensive or unavailable. In such case natural human arm postures have to be replicated autonomously. This challenge mainly results from the redundant degrees of freedom (DoFs) and unknown postural control strategy of human arms [6].

Recently, massive attention has been attracted to replicate natural human arm postures via building kinematic redundancy resolution criteria. Existing approaches mainly fall into two categories: model-based methods [7], [8], [9], [10], [11], [12], [13], [14] and data-driven methods [15], [16], [17], [18], [19], [20], [21]. For model-based methods, plausible kinematic redundancy resolution criteria are derived from the state variables of a simplified 7-DoF human arm model. Then, these criteria are optimized to replicate natural human arm postures. The involved variables usually include positions, velocities, accelerations, torques, lumped muscle forces and energy. While data-driven methods aim at building the regression relationship among certain posture-related parameters extracted from the tracked data of human arm motions. Then, the built relationship can be used to resolve the kinematic redundancy of human arms in a human-like fashion. Both the two categories of methods were reported to replicate natural human arm postures agreeing with their experimental data. However, on one hand, there is significant inconsistency between the simplified 7-DoF kinematic models and the state-of-the-art muscle-actuated model of human arms published in [22]. On the other hand, the empirical assumptions may lead the kinematic redundancy resolution criteria (e.g. fundamental functions or neural networks) not able to capture the actual physiological characteristics of natural human arm postures. As a result, existing kinematic redundancy resolution criteria

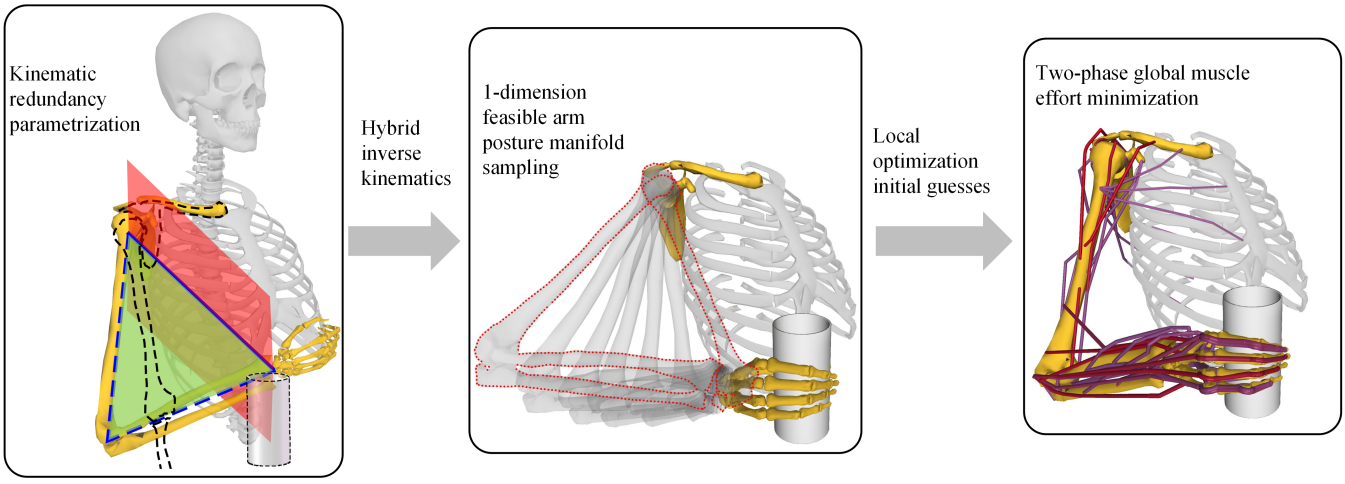

Fig. 1. The flowchart of the muscle-effort-minimization-inspired kinematic redundancy resolution for replicating natural human arm postures.

may result in objective functions mismatching the hypothesis set for fitting natural arm postures. Since a mismatched hypothesis set for learning will increase the generalization error bound [23], existing kinematic redundancy resolution criteria may suffer from limited generalization ability in replicating natural human arm postures across tasks.

In interactive scenarios, humans usually choose a preferred arm posture from an infinite number of possibilities to reach a hand pose compatible for the target object to be manipulated [12]. The economic choice in humans can be understood as a weighing of benefits (e.g., reward) against costs (e.g., effort, delay, risk), which leads to a preference for the behavioral option with the highest expected utility [24]. Moreover, recent studies have provided support for the hypothesis that the human brain shapes motor patterns to minimize muscle effort against external load [25]. Besides the two categories of methods mentioned above, recent studies also showed the biological potential to replicate natural human arm postures. Figueredo *et al.* [26] argued that muscular-informed metrics could allow for a better evaluation and a more general kinematic redundancy resolution criterion applicable across tasks. Demircan *et al.* [27] showed the practicality of a biology measure that encodes information about the musculoskeletal system of human arms. In [28] and [29], a natural human arm posture is considered to be the result of minimizing an index of muscular effort. However, Lamperti *et al.* [28] adopted a simplified 7-DoF arm model to estimate muscle efforts, which may contribute to a degraded estimation accuracy. And Demircan *et al.* [29] pays little attention to replicating natural human arm postures with desired hand poses, which is indispensable for a robot to mimic the way of humans to accurately perform a task in interactive scenarios.

To effectively replicate natural human arm postures across interactive tasks, a constrained muscular effort minimization problem is formulated to resolve the kinematic redundancy of human arms in this work. It is based on a high-fidelity human arm musculoskeletal model (HAMM) and considers the implicit constraint (desired hand pose) and the inequality constraints (range of joint motion). The adopted high-fidelity HAMM is modified from Saul *et al.* [30] as described by McFarland *et al.* [31]. It includes an updated range of motion at the shoulder, ligaments models representing the gleno-humeral and coracohumeral ligaments, and an updated muscle model [32] with force-length and tendon curves. Differing from a 7-DoF simplified arm model, the high-fidelity HAMM has 7 independent joints and 13 mimic joints with 50 muscle compartments crossing these joints. And it is the state-of-the-art model of the human arm musculoskeletal system. A mimic joint here is a joint whose coordinate value depends on the coordinates of other independent joints in the kinematic structure. This high-fidelity musculoskeletal structure may contribute to a high accuracy for muscle effort estimation. However, it also means that one has to handle the complicated inverse kinematics (IK) of the simultaneously redundant and underactuated kinematic chain.

With the high-fidelity HAMM, the desired hand pose can impose highly complicated constraints upon the addressed minimization. And the formulated constrained minimization can be in general nonconvex, consequently sensitive to initial guesses in iterative procedures. So, it is impracticable to solve it directly with existing gradient-based deterministic approaches or standard evolutionary algorithms. To address it, two specified numerical algorithms, the hybrid IK algorithm and the two-phase global optimization algorithm, are developed to find the global minimum effectively. The idea of this study is depicted in Figure 1. The main contribution of this work lies in the following aspects:

1) A muscle-effort-minimization-inspired approach was proposed to resolve the kinematic redundancy of human arms for replicating natural human arm postures given a desired hand pose. With a high-fidelity HAMM, the natural human arm posture was determined via minimizing the muscle effort defined by the total squared activations of the involved muscles. The minimization considered the implicit constraint (desired hand pose) and the inequality constraints (range of joint motion).
2) An efficient hybrid IK algorithm was proposed to calculate the feasible IK solutions for the simultaneously redundant and underactuated high-fidelity HAMM. Given an arm swivel angle, feasible arm postures for a desired hand pose can be determined through numerical

iterations with initial guesses deduced from the analytical IK solutions of a specific 7-DoF kinematic model.

3) A two-phase optimization algorithm was proposed to solve the nonconvex muscle-effort-minimization problem globally. Firstly, a local deterministic search was performed on the null-space of the geometric Jacobian matrix in each initial guess of arm posture to find potential local minimums. The initial guess candidates were generated using the proposed hybrid IK algorithm to achieve geometrical equidistance over the 1-dimension manifold of feasible arm postures. Secondly, a global search was performed to find the optimal solution of the nonconvex problem, which was based on an initial guess resampling strategy and the found local minimums.

This paper is organized in the following manner. In Section II, the muscle-effort-minimization problem is formulated. In Section III, synthetic analysis for solving the nonconvex minimization problem is performed. In Section IV, validation experiments and replication performance are demonstrated. Discussion is in Section V. Finally, the conclusion is summarized in Section VI.

II. Methodology

To replicate natural human arm postures when given a desired hand pose, we hereby address a constrained muscle-effort-minimization problem based on the high-fidelity HAMM. The general method consists of five parts, model assumptions, muscle effort minimization formulation, kinematic redundancy parametrization, hybrid IK algorithm, and two-phase global optimization algorithm.

A. Model Assumptions

For daily manipulation tasks, the voluntary human arm movement to manipulate an object can be divided into three stages, reaching, grasping, and manipulation [33]. Reaching movements are usually involved with visual feedback and motion speed, which contribute to a complex online neural and motor control [34]. Natural human arm movements were studied in our previous works [35]. In this work, our emphasis is laid on the grasping and manipulation stages where very low arm velocity and meticulous finger motions usually occur without significantly changing the arm posture. Consequently, the assumptions posed on the muscle effort minimization in this work can be as follows:

1) The inertial forces caused by negligible motions of the human arm and hand are ignored for the quasi-static arm postures in grasping and manipulation stages.
2) Gravitational loads acting on human arm joints are only caused by the gravity of the human arm and hand. The gravity of the task-dependent object is not taken into the minimization.
3) As reported by [36], moving and holding may be controlled by separate neural structures for skilled behaviors. In grasping and manipulation stages lasting a period of time, the natural human arm postures are only dependent on kinematic constraints and the gravitational loads. They don't depend on the motion that moved the upper limb to the current posture or the motion that will move the upper limb to next posture.

B. Muscle Effort Minimization Formulation

With the high-fidelity HAMM and a specific hand pose, the kinematic and dynamic equations of the HAMM can be expressed as

$$\begin{aligned} \boldsymbol{\tau} &= \mathbf{A}(\boldsymbol{q})\ddot{\boldsymbol{q}} + \boldsymbol{b}(\boldsymbol{q}, \dot{\boldsymbol{q}}) + \boldsymbol{g}(\boldsymbol{q}) \\ \mathbf{T}_e &= \boldsymbol{f}_e(\boldsymbol{q}) \\ \boldsymbol{q} &\le \boldsymbol{q}_{\mathrm{U}} \\ \boldsymbol{q} &\ge \boldsymbol{q}_{\mathrm{L}} \\ \boldsymbol{q} &\notin \aleph(\boldsymbol{q}) \end{aligned} \tag{1}$$

where $\boldsymbol{q} \in \mathbb{R}^{20\times 1}$ is the vector of generalized coordinates for the arm joints. $\mathbf{A}(\boldsymbol{q}) \in \mathbb{R}^{20\times 20}$ is the mass matrix. $\boldsymbol{b}(\boldsymbol{q}, \dot{\boldsymbol{q}}) \in \mathbb{R}^{20\times 1}$ is the vector of centrifugal and Coriolis terms. $\boldsymbol{g}(\boldsymbol{q}) \in \mathbb{R}^{20\times 1}$ is the vector of gravity terms. $\boldsymbol{\tau} \in \mathbb{R}^{20\times 1}$ is the vector of the generalized control forces (joint torques). $\mathbf{T}_{\mathrm{e}} \in \mathbb{R}^{4\times 4}$ is the pose matrix for the hand. $\boldsymbol{q}_{\mathrm{U}} \in \mathbb{R}^{20\times 1}$ is the upper limits of the generalized joint coordinates. $\boldsymbol{q}_{\mathrm{L}} \in \mathbb{R}^{20\times 1}$ is the lower limits. $\boldsymbol{f}_{\mathrm{e}}(\cdot) : \mathbb{R}^{20\times 1} \to \mathbb{R}^{4\times 4}$ is the continuous nonlinear forward-kinematics mapping for the HAMM. And $\aleph(\boldsymbol{q})$ is the subject-specific arm configuration set where collisions between the arm and thorax may occurs in actual experiments. For conciseness we will often refrain from explicitly denoting the functional dependence of the quantities on $\boldsymbol{q}$ and $\dot{\boldsymbol{q}}$.

Based on the calculated joint torques $\boldsymbol{\tau}$, the correspondence muscle activations $\boldsymbol{a}^{\mathrm{opt}}$ can be calculated by solving the following optimization [37]

$$\begin{aligned} \boldsymbol{a}^{\mathrm{opt}} &= \arg\min_{\boldsymbol{a}} \sum_{m=1}^{50} (a_m)^2 \\ \text{s.t. } \tau_j &= \sum_{m=1}^{50} a_m f\left(F_m^0, l_m, v_m\right) \cdot r_{m,j} \cos\alpha_m, \\ & \quad j = 1, \ldots, 20 \end{aligned} \tag{2}$$

where $\boldsymbol{a} \in \mathbb{R}^{50\times 1}$ denotes the activation levels of the 50 involved muscles. a_m, the mth element of $\boldsymbol{a}$, is the activation level of the mth muscle. F_m^0 is its maximum isometric force. l_m is its length. v_m is its shortening velocity. $f\left(F_m^0, l_m, v_m\right)$ is its force-length-velocity surface. $r_{m,j}$ is its moment arm about the jth joint axis. α_m is its pennation angle of the muscle. And τ_j, the jth component of $\boldsymbol{\tau}$, is the joint torque acting about the jth joint.

With the model assumptions, only the gravity of the arm and hand is taken into the minimization. And a natural human arm posture is considered to be the result of minimizing the index of the muscular effort among all the possibilities [25], [28], [29]. Therefore, the muscle-effort-minimization problem is formulated as minimization (3) with the total sum of squared muscle activations, where $l_m(\boldsymbol{q})$ and $r_{m,j}(\boldsymbol{q})$ are the posture-dependent muscle length and moment arm about the jth joint of the mth muscle, respectively. a_m^{opt} is the mth element of the $\boldsymbol{a}^{\mathrm{opt}}$ determined by minimization (2) with a certain $\boldsymbol{q}$ for arm joint coordinates. And $E(\boldsymbol{q})$ is the posture-dependent muscle effort to be optimized. $\boldsymbol{q}_{\mathrm{opt}}$ is the optimal posture that

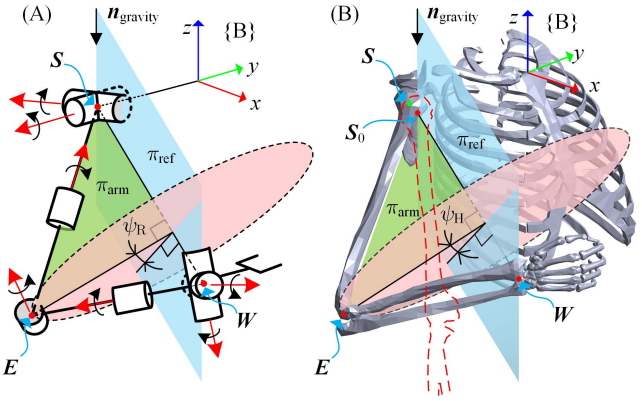

Fig. 2. Definitions of the arm swivel angle. (A) the arm swivel angle ψ_R used to parameterize the kinematic redundancy of common 7-DoF robotic arms. (B) the arm swivel angle ψ_H used to parameterize the kinematic redundancy of the HAMM. The shoulder joint center $\boldsymbol{S_0}$ in the home posture outlined by red dash-line is used to define the ψ_H.

minimizes $E(\boldsymbol{q})$.

$$
\begin{aligned}
&\boldsymbol{q}_{\text{opt}} = \arg\min_{\boldsymbol{q}} \; E(\boldsymbol{q}) \\
&\text{s.t. } E(\boldsymbol{q}) = \sum_{m=1}^{50} \left(a_m^{\text{opt}}\right)^2 \\
&\tau_j = \sum_{m=1}^{50} a_m^{\text{opt}} f\left(F_m^0, l_m(\boldsymbol{q}), 0\right) \cdot r_{m,j}(\boldsymbol{q}) \cos\alpha_m, \\
&j = 1, \ldots, 20 \\
&\boldsymbol{\tau} = \boldsymbol{g}(\boldsymbol{q}) \\
&\mathbf{T}_{\text{e}} = \boldsymbol{f}_{\text{e}}(\boldsymbol{q}) \\
&\boldsymbol{q} \le \boldsymbol{q}_{\text{U}} \\
&\boldsymbol{q} \ge \boldsymbol{q}_{\text{L}} \\
&\boldsymbol{q} \notin \aleph(\boldsymbol{q})
\end{aligned}
\tag{3}
$$

C. Kinematic Redundancy Parametrization

Since the high-fidelity HAMM has an intractable kinematic structure with 7 independent joints and 13 mimic joints, it is impractical to handle its IK directly in the joint configuration space. Fortunately, the high-fidelity HAMM shares a very similar physical form, a shoulder-elbow-wrist structure, with common 7-DoF robotic arms in spite of negligible posture-dependent displacements in shoulder joint center. Consequently, the kinematic redundancy of the HAMM can be parameterized geometrically by the arm swivel angle widely used in 7-DoF robotic arms.

As shown in Figure 2(A), the arm swivel angle ψ_R for common 7-DoF robotic arms is defined as the angle between the green arm plane $\boldsymbol{\pi}_{\text{arm}}$ and the blue reference plane $\boldsymbol{\pi}_{\text{ref}}$. The $\boldsymbol{\pi}_{\text{arm}}$ is spanned by the shoulder $\boldsymbol{S}$, elbow $\boldsymbol{E}$, and wrist $\boldsymbol{W}$. And the $\boldsymbol{\pi}_{\text{ref}}$ is spanned by the shoulder $\boldsymbol{S}$, wrist $\boldsymbol{W}$ and gravity vector $\boldsymbol{n}_{\text{gravity}}$. Mathematically, ψ_R can be given by

$$
\begin{aligned}
\psi_R = &\operatorname{sgn}\left((\boldsymbol{l}_{\text{SW}} \times \boldsymbol{l}_{\text{SE}}) \cdot \boldsymbol{n}_{\text{gravity}}\right) \\
&\cdot \operatorname{acos}\left(\frac{(\boldsymbol{l}_{\text{SW}} \times \boldsymbol{l}_{\text{SE}}) \cdot (\boldsymbol{l}_{\text{SW}} \times \boldsymbol{n}_{\text{gravity}})}{\|\boldsymbol{l}_{\text{SW}} \times \boldsymbol{l}_{\text{SE}}\| \cdot \|\boldsymbol{l}_{\text{SW}} \times \boldsymbol{n}_{\text{gravity}}\|}\right)
\end{aligned}
\tag{4}
$$

where $\boldsymbol{S}$, $\boldsymbol{E}$, $\boldsymbol{W}$ and $\boldsymbol{n}_{\text{gravity}}$ are vectors in $\mathbb{R}^{3\times1}$ represented in the base frame B of a 7-DoF robotic arm. $\operatorname{sgn}(\cdot)$ is the sign function and $\|\cdot\|$ is the L^2-Norm function. $\boldsymbol{l}_{\text{SW}}$ and $\boldsymbol{l}_{\text{SE}}$ are vectors in $\mathbb{R}^{3\times1}$ from $\boldsymbol{S}$ to $\boldsymbol{W}$ and $\boldsymbol{E}$, respectively.

As shown in Figure 2(B), $\boldsymbol{S}_0$ and $\boldsymbol{S}$ are the shoulder joint center in the home posture and in a specific arm posture, respectively. In this study, the arm swivel angle ψ_H for the HAMM is defined using the $\boldsymbol{S}_0$ instead of $\boldsymbol{S}$. It can achieve the consistency with the ψ_R for common 7-DoF robotic arms and the geometric computation efficiency on the 1-dimension manifold of feasible arm postures. And ψ_H can be given by

$$
\begin{aligned}
\psi_H = &\operatorname{sgn}\left((\boldsymbol{l}_{\text{S}_0\text{W}} \times \boldsymbol{l}_{\text{S}_0\text{E}}) \cdot \boldsymbol{n}_{\text{gravity}}\right) \\
&\cdot \operatorname{acos}\left(\frac{(\boldsymbol{l}_{\text{S}_0\text{W}} \times \boldsymbol{l}_{\text{S}_0\text{E}}) \cdot (\boldsymbol{l}_{\text{S}_0\text{W}} \times \boldsymbol{n}_{\text{gravity}})}{\|\boldsymbol{l}_{\text{S}_0\text{W}} \times \boldsymbol{l}_{\text{S}_0\text{E}}\| \cdot \|\boldsymbol{l}_{\text{S}_0\text{W}} \times \boldsymbol{n}_{\text{gravity}}\|}\right)
\end{aligned}
\tag{5}
$$

where $\boldsymbol{S}_0$, $\boldsymbol{E}$ and $\boldsymbol{W}$ are vectors in $\mathbb{R}^{3\times1}$ represented in the base frame B of the HAMM. $\boldsymbol{l}_{\text{S}_0\text{W}}$ and $\boldsymbol{l}_{\text{S}_0\text{E}}$ are vectors in $\mathbb{R}^{3\times1}$ from $\boldsymbol{S}_0$ to $\boldsymbol{W}$ and $\boldsymbol{E}$, respectively.

With the defined ψ_H for parametrizing the kinematic redundancy of the HAMM geometrically, different feasible arm postures for a desired hand pose can be compared using the arm swivel angle approximately but efficiently. Also, interpolations for the feasible postures of the HAMM can be performed in a joint-coordinate-invariant geometric manner (interpolation in the range of the arm swivel angle) in spite of the negligible motion of the shoulder $\boldsymbol{S}$. As a result, the original complicatedly constrained nonconvex minimization (3) can be transformed into a nonconvex minimization with a bounded constraint over the arm swivel angle. It can be given by

$$
\begin{aligned}
&\boldsymbol{q}_{\text{opt}} = \arg\min_{\boldsymbol{q}} \; E(\boldsymbol{q}) \\
&\text{s.t. } \psi_L \le \psi_H(\boldsymbol{q}) \le \psi_U, \quad \boldsymbol{q} \in \wp
\end{aligned}
\tag{3.1}
$$

where $\wp$ is the 1-dimension manifold of feasible arm postures satisfying the desired hand pose and ranges of joint motion. ψ_L and ψ_U are the lower and upper limit of ψ_H, respectively.

D. Hybrid IK Algorithm

With ψ_H for the kinematic redundancy parametrization, the addressed minimization can be transformed from minimization (3) to minimization (3.1). Beneficially, this transformation simplifies the complicated constraints into a simple 1-dimensional search space over the arm swivel angle ψ_H. To get the global solution of minimization (3.1), the 1-dimension feasible posture manifold $\wp$ need to be calculated with regards to feasible range of ψ_H. Therefore, an efficient IK procedure is needed to compute the joint coordinates $\boldsymbol{q}$ for an arm posture when given an arm swivel angle ψ_H and a hand pose. This IK procedure need help to obtain enough geometrically equidistant initial guess candidates over $\wp$. And then, the global minimum may be reached from at least one of the candidates probably.

However, the IK calculation can be a daunting computational exercise when it comes to the simultaneously redundant and underactuated high-fidelity HAMM [38]. To address it, a hybrid IK algorithm is developed by combining an analytical

TABLE I
LINK PARAMETERS OF THE SPECIFIC 7-DOF KINEMATIC MODEL

i	α_{i-1} (rad)	a_{i-1} (m)	θ_i (rad)	d_i (m)
1	0	α_0	θ_0	0
2	$\pi/2$	0	0	0
3	$-\pi/2$	0	$\pi/2$	$-d_{se}$
4	$\pi/2$	0	0	0
5	$-\pi/2$	0	0	$-d_{ew}$
6	$-\pi/2$	0	$\pi/2$	0
7	$\pi/2$	0	0	0

α_{i-1} , a_{i-1} , θ_i and d_i are the Denavit-Hartenberg parameters following Craig's convention. α_0 and θ_0 are constants to ensure identical base configuration with the scaled HAMM. d_{se} and d_{ew} are the lengths of the upper arm and the forearm, respectively.

IK procedure for a specific 7-DoF kinematic model and a numerical IK procedure based on the geometric Jacobian matrix for the high-fidelity HAMM. Derived from the high-fidelity HAMM, the specific 7-DoF kinematic model has a similar shoulder-elbow-wrist structure and equivalent lengths of the upper arm and forearm. Its initial parameters are given in Table I. Also, the kinematic redundancy for the specific 7-DoF kinematic model is parametrized with the arm swivel angle ψ_S.

Given a hand pose $\mathbf{T}_e$ and an arm swivel angle ψ_S, the IK solution $\boldsymbol{q}^s \in \mathbb{R}^{7\times1}$ for the specific 7-DoF kinematic model can be calculated analytically in position domain [39]. Benefiting from the similarity in kinematic structure, $\boldsymbol{q}^s$ can be transformed to initial guess $\boldsymbol{q}_{init} \in \mathbb{R}^{20\times1}$ for the numerical IK procedure for the high-fidelity HAMM. The rule for transforming $\boldsymbol{q}^s$ to $\boldsymbol{q}^{ind}_{init} \in \mathbb{R}^{7\times1}$, the initial guess of the independent coordinates for the high-fidelity HAMM, is given by

$$\boldsymbol{q}^{ind}_{init} = \mathbf{K}\boldsymbol{q}^s \tag{6}$$

where $\mathbf{K}$ is a sparse matrix given by

$$\mathbf{K} = \begin{bmatrix} 1 & & & & \\ & 1 & & & \\ 1 & & 1 & & \\ & & & \mathbf{I}_{4\times4} & \end{bmatrix}$$

And the $\boldsymbol{q}_{init}$ can be given by

$$\boldsymbol{q}_{init} = \mathbf{W}\boldsymbol{q}^{ind}_{init} \tag{7}$$

where $\mathbf{W} \in \mathbb{R}^{20\times7}$ is the weight matrix that transforms the independent coordinates of the HAMM $\boldsymbol{q}^{ind} \in \mathbb{R}^{7\times1}$ to its generalized coordinates $\boldsymbol{q} \in \mathbb{R}^{20\times1}$. With the obtained $\boldsymbol{q}_{init}$, the well-known numerical technique Levenberg–Marquardt (LM) is used with the geometric Jacobian matrix to calculate the accurate IK solution $\boldsymbol{q}_{refined} \in \mathbb{R}^{20\times1}$ that belongs to $\wp$.

E. Two-Phase Global Optimization Algorithm

Since the hand pose is involved with the forward- kinematic of the high-fidelity HAMM, the formulated muscle effort minimization (3) is in general nonconvex and possesses local minimums. The number and properties of the local minimums are strongly influenced by the desired hand pose $\mathbf{T}_e$. As a result, it is impracticable to solve the constrained nonconvex muscle-effort-minimization problem directly with existing gradient-based deterministic approaches or standard evolutionary algorithms. Hereby, a two-phase algorithm is developed in this work, which consists of a local-search phase and a global-search phase. As mentioned before, the $\wp$ of the high-fidelity HAMM is parametrized by the arm swivel angle ψ_H when given a desired hand pose $\mathbf{T}_e$. It is also called null-space or self-motion manifold [40]. Therefore, using the proposed hybrid IK algorithm, the $\wp$ can be sampled over the admissible range of ψ_H to generate geometrically quasi equidistant initial guess candidates for the two-phase search.

In the local-search phase, minimization (3.1) is addressed locally with an iterative procedure. For each arm joint configuration $\boldsymbol{q}$ in the initial guess candidates, the local search step $\boldsymbol{d}$ is given by

$$\begin{aligned} \boldsymbol{d} &= \begin{cases} \rho\boldsymbol{n} & if\ (E(\boldsymbol{q}+\rho\boldsymbol{n}) - E(\boldsymbol{q})) < 0 \\ -\rho\boldsymbol{n} & if\ (E(\boldsymbol{q}-\rho\boldsymbol{n}) - E(\boldsymbol{q})) < 0 \end{cases} \\ \boldsymbol{n} &= \frac{\mathbf{W}\delta\boldsymbol{q}^{ind}}{\left\|\mathbf{W}\delta\boldsymbol{q}^{ind}\right\|} \\ \delta\boldsymbol{q}^{ind} &\in N(\boldsymbol{J}_v(\boldsymbol{q})\mathbf{W}) \end{aligned} \tag{8}$$

where $\boldsymbol{q}^{ind} \in \mathbb{R}^{7\times1}$ is the independent coordinates of the high-fidelity HAMM. $\delta\boldsymbol{q}^{ind} \in \mathbb{R}^{7\times1}$ is the step direction in the null-space. $\boldsymbol{J}_v(\boldsymbol{q}) \in \mathbb{R}^{6\times20}$ is the so-called geometric Jacobian matrix. $N(\cdot)$ is the null-space of a matrix. And the step size ρ is a positive and adaptable variable which is set to decrease the muscle effort $E(\boldsymbol{q})$. In addition, we assume that $\boldsymbol{q}$ is not a singular joint configuration. Hence $\boldsymbol{J}_v(\boldsymbol{q})\mathbf{W} \in \mathbb{R}^{6\times7}$ is full row rank and $N(\boldsymbol{J}_v(\boldsymbol{q})\mathbf{W})$ is a vector space of 1 dimension. The stopping criterion for the local search is given by

$$\rho < \kappa \tag{9}$$

where κ is a specific constant.

In the global-search phase, the "best" local minimum among the earlier found local minimums is selected as the global minimum. However, whether the found local minimums cover the global minimum is strongly dependent on the number of the generated geometrically quasi equidistant initial guess candidates in the $\wp$. Therefore, resampling with a higher density in the $\wp$ is performed to repeat the local-search phase till the stopping rule for the global search is met. The possible stopping rules for the global search are as follows [41].

1) The posterior expectation of the number of local minima

$$\frac{\omega(M-1)}{M-\omega-2} < \omega + \varepsilon \tag{10}$$

2) The posterior expected relative size of the non-observed regions of attraction

$$\frac{\omega(\omega+1)}{M(M-1)} < \delta \tag{11}$$

where ω is the number of different local minimums discovered. M is the number of initial guess candidates applied in the local-search phase. ε and δ are the specific stopping criteria.

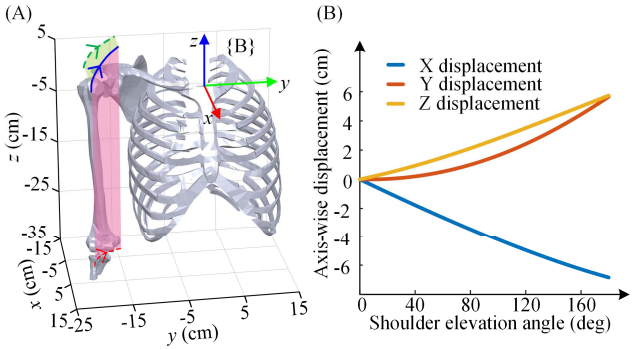

Fig. 3. Motion of the glenohumeral joint center $\boldsymbol{S}$ with regards to the shoulder elevation angle ranging from 0 to 180 degrees. (A) the blue arrowed curve denotes the motion of human glenohumeral joint center $\boldsymbol{S}$. The green and red dashed arrowed curve denote the projections onto the back plane and bottom plane, respectively. (B) The axis-wise displacement of $\boldsymbol{S} - \boldsymbol{S}_0$ with regards to the shoulder elevation angle.

III. Synthetic Analysis

In this section, synthetic analysis is performed to evaluate the performance of the kinematic redundancy parametrization, the hybrid IK algorithm and the two-phase global optimization algorithm. With the high-fidelity HAMM, results of the numerical analysis are demonstrated.

A. Arm Swivel Angle Modeling Disagreement

In the high-fidelity HAMM, the glenohumeral joint center $\boldsymbol{S}$ shifts according to the motions of the clavicle and the scapula relative to the body base frame. And the motion of $\boldsymbol{S}$ only depends on the shoulder elevation angle represented by q_2^{ind} (ranging from 0 to 180 degrees) in the HAMM as shown in Figure 3(A). While in common 7-DoF robotic arms with a spherical-revolute-spherical structure, the shoulder joint center keeps fixed in their base frame. As described in the section Kinematic Redundancy Parametrization, the ψ_{H} for the HAMM is defined using the shoulder $\boldsymbol{S}_0$ in its home posture in this study. And the axis-wise displacement ($\boldsymbol{S}$ - $\boldsymbol{S}_0$) is shown in Figure 3(B).

From the synthesized analysis results shown in Figure 3, the displacement of the glenohumeral joint center $\boldsymbol{S}$ relative to the reference $\boldsymbol{S}_0$ increases with the shoulder elevation angle. When the shoulder elevation angle reaches its upper limit 180 degrees, the largest displacement occurs ($-$6.8cm, 5.7 cm and 5.7cm in x, y and z direction, respectively). This shoulder-elevation-angle-dependent displacement can lead to a disagreement in the arm swivel angle modeling. And a larger shoulder elevation angle implies a more considerable modeling disagreement.

To quantitively evaluate the arm swivel angle modeling disagreement, the actual human arm swivel angle ψ_{H}^* is derived with $\boldsymbol{S}, \boldsymbol{E}, \boldsymbol{W}$ and $\boldsymbol{n}_{\text{gravity}}$ as shown in Figure 2(B). It is similar to the definition of ψ_{H}. So, the modeling disagreement with regards to the shoulder elevation angle can be obtained over the feasible arm posture manifold of a certain hand pose. Without loss of generality, the hand pose compatible for holding a vertical cup in front of the human is chosen to evaluate the arm swivel angle modeling disagreement, which has a relatively wide range of self-motion. The modeled and actual arm swivel angle with regards to the shoulder elevation angle is shown in Figure 4(A). And the disagreement over ψ_{H} and ψ_{H}^* is depicted in Figure 4(B).

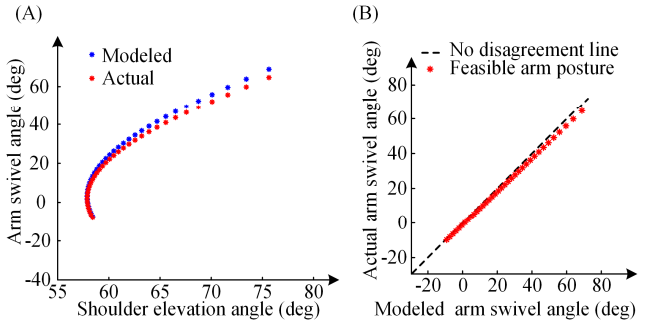

Fig. 4. Arm swivel angle for the feasible arm postures given a certain hand pose. (A) the modeled arm swivel angle ψ_{H} and actual arm swivel angle ψ_{H}^* with regards to the shoulder elevation angle. (B) the arm swivel angle modeling disagreement.

With the synthesis analysis, the modeling disagreement of the arm swivel angle, $\left|\psi_{\text{H}} - \psi_{\text{H}}^*\right|$, is 2.16±1.02 degrees for the hand pose with a self-motion range of 74.3 degrees. The correspondence elbow position disagreement in the high-fidelity HAMM caused by this modeling disagreement can be given by

$$\delta\boldsymbol{E} = \left(\psi_{\text{H}} - \psi_{\text{H}}^*\right) \cdot \frac{(\boldsymbol{l}_{\text{SE}} \times \boldsymbol{l}_{\text{SW}})}{\|\boldsymbol{l}_{\text{SW}}\|} \tag{12}$$

where $\boldsymbol{S}$, $\boldsymbol{E}$ and $\boldsymbol{W}$ are vectors in $\mathbb{R}^{3\times1}$ represented in the base frame B of the high-fidelity HAMM. And $\delta\boldsymbol{E}$ is the elbow position disagreement with the two arm swivel angles ψ_{H} and ψ_{H}^*. With an average upper arm length of 29cm ($\boldsymbol{l}_{\text{SE}}$) [30], the maximum magnitude of the $\delta\boldsymbol{E}$ is 0.77cm with a common forearm and upper arm angle of 90 degrees. It is at a negligible scale compared to the self-motion scale of more than 26cm. Also, compared with the reported arm swivel angle prediction error of 5 degrees [12], the arm swivel angle modeling disagreement is acceptable to some extent.

B. Posture Uncertainty in the Hybrid IK Algorithm

Due to kinematic redundancy in the high-fidelity HAMM, there are infinite optional LM step vector for computing the $\boldsymbol{q}_{\text{refined}}$ in the numerical part of the proposed hybrid IK algorithm without an additional constraint. However, a general constraint will somewhat pose posture uncertainty (arm swivel angle variation) in approaching the desired hand pose $\mathbf{T}_{\text{e}}$. It means generating IK solutions for the HAMM which are not equidistant over the 1-dimension manifold of feasible arm postures. Since the $\boldsymbol{q}_{\text{init}}$ is already close to an accurate IK solution and the elevation of the elbow depends only on the shoulder elevation angle, we choose to fix the generalized coordinates related to independent coordinate q_2^{ind} and q_4^{ind} by turns in LM iterations for a balance of efficiency and complexity. The hybrid IK algorithm is summarized in Table II.

And the posture uncertainty is measured by

$$e_\psi = \psi_S - \psi_{\text{H}} \tag{13}$$

To quantitively evaluate the posture uncertainty resulted from the hybrid IK algorithm, a set of hand poses across the

TABLE II
HYBRID IK ALGORITHM

Algorithm 1. The Hybrid IK algorithm for the HAMM

Input: the HAMM, the desired hand pose $\mathbf{T}_e$, the arm swivel angle interval $\delta\psi_S$

I) Analytical part

1) generate geometrically equidistant samples ψ_S from the whole range of arm swivel angle to a set Ψ_S with an interval of $\delta\psi_S$

2) set the IK solution set Q^s for the specific 7-DoF model to empty

for each ψ_S in Ψ_S

Compute the IK solution $\boldsymbol{q}^s$ for the specific 7-DoF model with $\mathbf{T}_e$ and ψ_S using the analytical IK solver.

Insert newly computed IK solution $\boldsymbol{q}^s$ to Q^s.

end for

II) Numerical part

3) set IK solution set $Q_{refined}$ for the HAMM to empty

for each $\boldsymbol{q}^s$ in Q^s

$\boldsymbol{q}_{init}^{ind} \leftarrow \mathbf{K}\boldsymbol{q}^s$ as equation (6)

$\boldsymbol{q}_{init} \leftarrow \mathbf{W}\boldsymbol{q}_{init}^{ind}$ as equation (7)

compute the accurate IK solution $\boldsymbol{q}_{refined}$ using the LM algorithm with $\boldsymbol{q}_{init}$ and $\mathbf{T}_e$

if $\boldsymbol{q}_{refined} \le \boldsymbol{q}_U$ **and** $\boldsymbol{q}_{refined} \ge \boldsymbol{q}_L$ **and** $\boldsymbol{q}_{refined} \notin \aleph(\boldsymbol{q})$ **then**

insert newly computed IK solutions $\boldsymbol{q}_{refined}$ to $Q_{refined}$.

end if

end for

Output: quasi geometrically equidistant feasible IK solutions set $Q_{refined}$ for the HAMM

reachability space are collected for the synthesis analysis. They are compatible for holding a vertical cup with a relatively large range of self-motion. And the synthesized posture uncertainty is shown in Figure 5(A). The performance of the proposed hybrid IK algorithm for the HAMM is evaluated by the position and orientation errors between the desired hand pose $\mathbf{T}_e$ and the calculated hand poses with joint configurations of $\boldsymbol{q}_{init}$ and $\boldsymbol{q}_{refined}$. The position and orientation errors are shown in Figure 5(B) and 5(C), respectively.

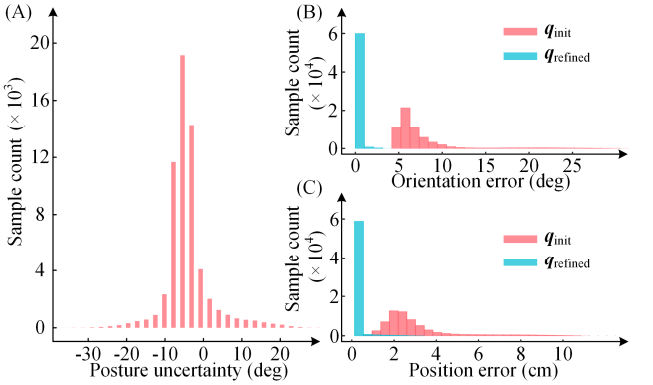

Fig. 5. Performance of the proposed hybrid IK algorithm for the high-fidelity HAMM. (A) the posture uncertainty $(\psi_S - \psi_H)$across the daily task space. (B) and (C) show position and orientation errors between the desired hand pose $\mathbf{T}_e$ and the hand poses with joint configurations of $\boldsymbol{q}_{init}$ and $\boldsymbol{q}_{refined}$, respectively.

TABLE III
GLOBAL OPTIMIZATION ALGORITHM

Algorithm 2. The Two-Phase Global Optimization Algorithm

Input: the HAMM, the desired hand pose $\mathbf{T}_e$, the arm swivel angle interval $\delta\psi_S$

Initialization

1) set the found local minimums Q_{local} to empty

2) generate the geometrically quasi equidistant feasible IK solutions set $Q_{refined}$ using **Algorithm 1** with the HAMM, the desired hand pose $\mathbf{T}_e$, the arm swivel angle interval $\delta\psi_S$.

I) local search phase

3) **for** each newly added $\boldsymbol{q}$ in $Q_{refined}$

initialize the step size ρ to a specific value

do

solve equations (1), (2) and (8) to obtain local search step $\boldsymbol{d}$, muscle effort $E(\boldsymbol{q})$, $E(\boldsymbol{q}-\boldsymbol{d})$ and $E(\boldsymbol{q}+\boldsymbol{d})$

if $E(\boldsymbol{q})$ is between $E(\boldsymbol{q}-\boldsymbol{d})$ and $E(\boldsymbol{q}+\boldsymbol{d})$

$\boldsymbol{q} \leftarrow \boldsymbol{q}+\boldsymbol{d}$

else

$\rho \leftarrow \rho/2$

end if

while stopping criterion (9) is not met

if $\boldsymbol{q}$ is not **in** Q_{local}

insert newly found local minimizer $\boldsymbol{q}$ to Q_{local}

end if

end for

II) global search phase

4) **if** stopping criterion (10) or (11) is not met

$\delta\psi_S \leftarrow \delta\psi_S/2$

generate new more samples using **Algorithm 1** and insert them to $Q_{refined}$

go to step (3) in **local search phase**

else

assign the "best" minimum in Q_{local} to $\boldsymbol{q}_{opt}$

end if

Output: the feasible arm posture $\boldsymbol{q}_{opt}$ reaching the global minimum of $E(\boldsymbol{q})$

C. Convergence of the Two-Phase Global Optimization

With the generated geometrically quasi equidistant feasible arm postures for minimization (3.1), the proposed two-phase global optimization algorithm to find the global minimum is summarized in Table III.

Due to the nonconvexity of the muscle-effort-minimization problem in minimization (3.1), the convergence of the proposed two-phase global optimization algorithm can be affected by the configurations of the user-defined variable $\delta\psi_S$, ρ, κ, ε and δ. Specifically, smaller $\delta\psi_S$, ρ, κ, ε and δ can improve the convergence to the global optimal at the expense of heavier computation load. Taking intrinsic variation of human arm postures into consideration, $\delta\psi_S$ is assigned with 2 degree in this study. Using the global stopping criterion (11), ρ, κ, ε and δ are assigned with 0.05, 0.01, 0.1 and 0.1, respectively. In this study, problem (1) and (2) with the HAMM are solved using the open-source software OpenSim [42]. Given the hand pose as in the section Arm Swivel Angle Modeling Disagreement, the convergence of $E(\boldsymbol{q})$ with regard to feasible arm joint

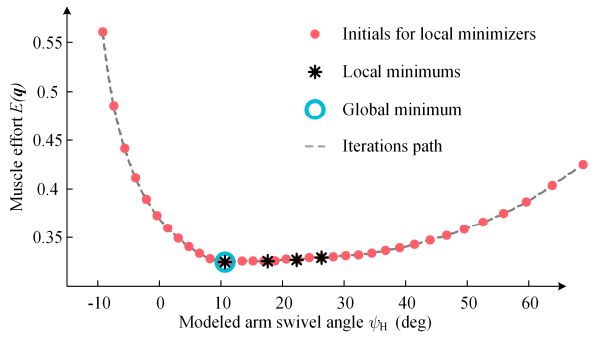

Fig. 6. Convergence of the proposed two-phase global optimization algorithm in solving the nonconvex muscle effort minimization.

configuration $\boldsymbol{q}$ parametrized by ψ_{H} is shown in Figure 6. And it implies that there are probably finite local minimums for the nonconvex minimization (3.1). With enough geometrically quasi equidistant initial guess candidates over the $\wp$, the global minimum will probably be reached from at least one of the candidates.

IV. Validation Experiments

Since the muscle-effort-minimization problem (3) considers the joint limits and hand pose with minor modeling assumptions, the proposed approach to replicating natural human arm postures has the potential to be applicable across daily task space. In this section, validation experiments are conducted to verify this potential.

A. Human Data Collection

To evaluate the performance of the proposed approach to replicating natural postures of human arms, demonstration data of human arms is collected in representative tasks. Without loss of generality, we choose holding an imaginary vertical cup at different positions within the reachability space of a subject's arm as the experimental tasks. And the basic idea is to evaluate the disagreement over the subject's natural arm postures and the replicated natural human arm postures with the scaled HAMM and the same hand poses. Since the admissible range of arm swivel angles is strongly dependent on hand poses, we choose experimental positions where the scaled HAMM has a relatively large admissible range. It can help to avoid the small misleading disagreements due to a limited range of the arm swivel angle. Finally, 114 points experimental locations are chosen, where the HAMM have an admissible arm swivel angle range larger than 40 deg. These locations are evenly distributed in the reachability space with an interval of 5 cm along each axis of the scaled HAMM base frame.

As shown in Figure 7, the 6-DoF robotic arm (Universal Robots, Denmark) is programmed to move the imaginary vertical cup, a vertical cylinder with locating slots for fingers, to each of the experimental locations. At each experimental trial, one right-handed subject is requested to slowly approach the imaginary vertical cup and then surround it in a grasping pattern for a period of time without interaction forces. When the subject has adjusted his arm to the most comfortable and effortless posture, the arm posture data is collected as a valid sample for the following verification.

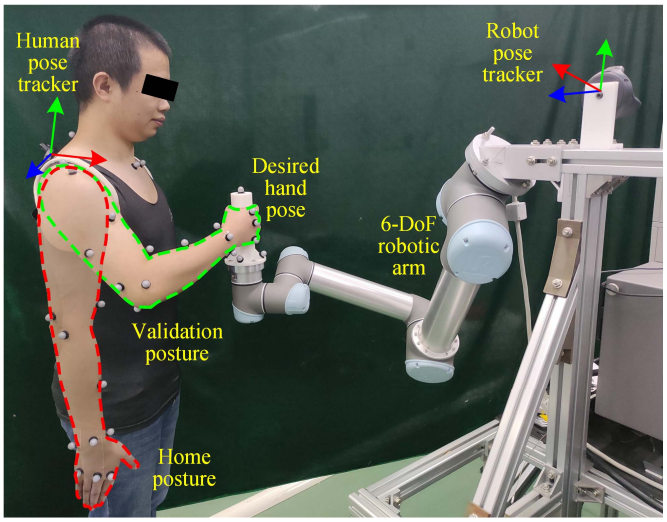

Fig. 7. The validation experiment setup.

In the experimental trials, human demonstration data is collected using the motion capture system (Vicon Motion Systems Ltd., U.K.). Two 6-dimension pose trackers (VIVE, U.S.), the human pose tracker and robot pose tracker, are used to compensate for the shift motion of the human body relative to the robotic arm. This can help to make the experimental trials at the expected locations. And the arm posture data of five right-handed subjects are collected for the following verification.

B. Performance Verification

The performance of the proposed approach is evaluated by the difference between the natural and the replicated arm swivel angles. By transforming the subjects' demonstration data into their body frame as shown in Figure 2(B), the subject-dependent scaling factors and correspondence arm joint coordinates are estimated via the scaling and IK module in OpenSim [42]. Based on the estimated arm joint configurations, the natural arm swivel angle at each of the experimental locations is calculated with the subject-dependent scaled HAMM. Correspondently, the replicated natural human arm posture is obtained by solving the proposed muscle effort minimization (3.1) with the subject-dependent scaled HAMM, the same hand pose, and the subject-dependent joint limits. And then the replicated natural arm postures are used to calculate the replicated arm swivel angles.

Since the admissible range of the arm swivel angle is hand-pose-dependent, we choose to use the absolute error of the arm swivel angle instead of the relative one to evaluate the performance of replicating natural human arm postures. It is more sensitive and meaningful to humans. Consequently, the performance is measured by the arm swivel angle replication error $\delta\psi$ given by

$$\delta\psi = \frac{1}{n}\sum_{i=1}^{n}\left|\psi_{\mathrm{H}\_i} - \psi_{\mathrm{H}\_i}^{\mathrm{natural}}\right| \tag{14}$$

where n is the number of trials taken into the verification. $\psi_{\mathrm{H}\_i}^{\mathrm{natural}}$ is the natural human arm swivel angle in the

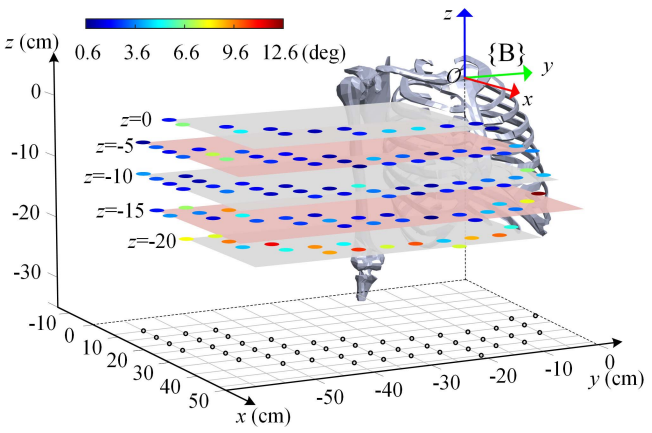

Fig. 8. The mean arm swivel angle replication errors at each of the 114 experimental locations of the five right-handed subjects. The coordinates of experimental locations are represented in the body base frame B defined in previous section. Black circles on the bottom plane are the vertical projections of the 114 points for experimental trials.

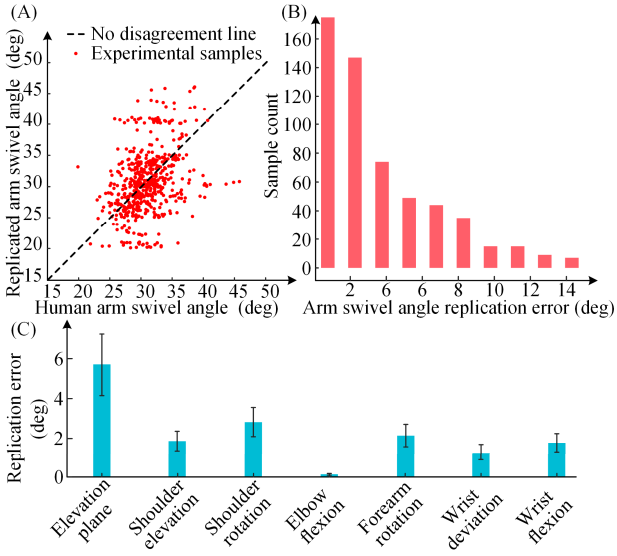

Fig. 9. Replication errors of all the experimental trials of five subjects at 114 locations. (A) the disagreement over the natural human arm swivel angle and the replicated arm swivel angle given the same hand pose. (B) the histogram of the arm swivel angle replication errors across all experimental trials. (C) coordinate-wise replication errors (mean and standard deviation) of the 7 independent joints in HAMM.

ith experiment trial and ψ_{H_i} is the correspondence arm swivel angle of the replicated natural human arm posture $\boldsymbol{q}_{\mathrm{opt}}$. Both $\psi_{\mathrm{H}\_i}^{\mathrm{natural}}$ and ψ_{H_i} are defined according to the ψ_{H} in the section Kinematic Redundancy Parametrization. A small value of $\delta\psi$ indicates good replication.

In Figure 8, the averaged arm swivel angle replication errors are depicted for each of the experimental locations across all subjects. The results suggest that the proposed approach for replicating natural human arm posture has the potential to be applicable across the daily task space. Because the arm swivel angle replication errors are acceptable at most experimental locations. Meanwhile, replication errors can be different among the experimental trails at different locations. In this study, the task for verification is holding an imaginary vertical cup at programmed positions. As shown in Figure 8, a verification test can achieve a good replication performance with a hand elevation similar to the right shoulder center. When the experiment trial is far below the right shoulder center, the wrist joints usually approach their joint limits and the replication performance can be significantly worse. It is probably due to the very limited ranges of motion in wrist joints as well as the insufficient modeling of subject-specific joint characteristics. As a result, the spatial distribution of the replication performance can be dependent on both the hand orientation and task position. And more accurate modeling of subject-specific joint characteristics may allow for a better replication performance across tasks with different hand poses.

Results in Figure 9 (A) and (B) show the statistics of the replication of the arm swivel angle. And the averaged replication error of arm swivel angle is 3.73±3.27 degree., compared with the reported arm swivel angle prediction error of 5 degrees [12]. In Figure 9 (C), the coordinate-wise replication errors are shown. As the human arm and the HAMM have a structure similar to spherical-revolute-spherical 7-DoF robots, the coordinate Elbow flexion is mainly related with the distance between the wrist and the shoulder given a desired hand pose. As a result, its replication error is independent from the kinematic redundancy resolution and can be very small in most cases. Since replication error of the arm swivel angle can significantly influence the position of the elbow, coordinates like Elevation plane, Shoulder elevation, Shoulder rotation, Forearm rotation, Wrist deviation and Wrist flexion are much more vulnerable to poor replication.

The performance verification of the proposed algorithms is conducted on a laptop computer (AMD R7 3750H and 8G RAM) with a system of Linux distribution (Ubuntu 18.04). With a specific configuration of $\mathbf{T}_{\mathrm{e}}$ and ψ_S, the time cost of the hybrid IK is 1.7±0.2 ms. And the time cost of the two-phase global minimization algorithms is 794±89 seconds for a specific $\mathbf{T}_{\mathrm{e}}$. And the C++ source codes for the proposed hybrid IK and two-phase global minimization algorithms are available in our repository (https://github.com/et0803/memikrr).

C. Performance Comparison

For performance comparison, studies that have explicitly reported the arm swivel angle errors in replicating natural human arm postures are revisited and summarized hereby. As shown in Table IV, most existing studies try to replicate natural human arm postures using a 7-DoF simplified kinematic model similar to human arms along with certain assumptions. However, the modeling assumptions inconsistent with the actual muscle-actuated model of human arms may lead to replication performance decay across tasks. As an alternative, the proposed muscle-effort-minimization-inspired approach can reach a comparable replication accuracy with the high-fidelity HAMM and minor assumptions. Benefiting from the modeling consistency and the biologically meaningful kinematic redundancy criterion, the proposed method may have better generalization ability in the reachability space of human arms.

TABLE IV
PERFORMANCE COMPARISON BY REPLICATION ERROR

	Replication error (deg)	Major modeling assumptions
This work	3.73±3.27	The high-fidelity HAMM [30]; muscle effort minimization [27].
Li et al. [11]	<5 (73% trails) >10 (3% trials)	7-DoF simplified robot model; 3 kinematic and 2 dynamic criteria; 2 synthesized criteria.
Kim et al. [12]	< 5	7-DoF simplified robot model; maximizing manipulability on the virtual trajectory.
Wu et al. [14]	3.94~17.06	7-DoF simplified robot model; shoulder, elbow, wrist, and mouth being coplanar.
Zanchettin et al. [15]	< 9	7-DoF simplified robot model; nonlinear relationship between hand pose and swivel angle.

Data are mean ± standard deviation or otherwise specified.

V. DISCUSSION

For robotic arm-hand systems, a hot topic is to perform manipulation tasks with human-like arm postures in an environment with human nearby [1], [2]. Therefore, replicating natural human arm postures autonomously is of significant importance when an accurate human demonstration is expensive or unavailable. Differing from the previous studies, this work presented a novel muscle-effort-minimization-inspired kinematic redundancy resolution for replicating natural human arm postures given desired hand poses. In the proposed method, benefits come at the expenses. Nevertheless, it may still be a particularly promising alternative for replicating natural human arm postures.

As for the benefits, a more convincing and biologically meaningful criterion, the muscle effort minimization, was built to resolve the kinematic redundancy of human arms. With the evidence that the human brain shapes motor patterns to minimize muscle effort against external load [25], the muscle effort minimization may be a fundamental principle for humans to make economic choices in daily behaviors [24]. As a result, the built criterion can allow for a better evaluation and a better generalization ability across tasks [26]. Compared with the existing studies, the adopted high-fidelity HAMM [30] is state of the art and far more consistent with human arms. It may produce less modeling and replication errors. Also, the built criterion has the potential to contribute to understanding the principles for natural human arm postures in moving case, where both online neural and motor control are involved [34].

As for the expenses, difficulties and relatively high computation load were induced by the high-fidelity HAMM in handling the constrained minimization objective for precise muscle effort estimation. Since the high-fidelity HAMM consists of 7 independent and 13 mimic joints [30], it is a daunting computational exercise to obtain the feasible arm postures and the "best" arm posture given a desired hand pose. While the existing studies can replicate natural human arm postures efficiently even analytically given a desired hand pose and a 7-DoF simplified kinematic model [11], [12], [14], [15]. Using the built criterion or identified relationship, they can achieve an acceptable replication accuracy and generalization ability. Fortunately, the hybrid IK algorithm and the two-phase global optimization algorithm proposed in this study can be used to solve the constrained and nonconvex minimization problem effectively and efficiently.

As for limitations, the proposed method for replicating natural human arm postures is strongly dependent on the accuracy of musculoskeletal system modeling of human arms. Disagreements over the high-fidelity HAMM and the actual muscle-actuated model of human arms may lead to significant disagreements over the replicated natural postures and the real human natural postures. Although the modeling assumptions in this study is minor, improvement on replication performance can be achieved if special further attention is paid to eliminating them. Firstly, comparable inertial loads caused by limited arm movements can challenge the first quasi-static assumption. However, these inertial loads can be taken into minimization (3) as shown in equation (1) to eliminate this assumption if there is an accurate estimation of the velocity and acceleration of the arm. Secondly, the gravity of the task-dependent object can also be taken in to minimization (3) to eliminate the second assumption if the weight of the object is known in a manipulation task. This assumption was only made for the verification experiments whose positions are controlled by a robotic arm. The third assumption was made for replicating the quasi-static arm postures in grasping and manipulation lasting a period of time. As reported in [36], there may be significant difference in the mechanisms of static arm posture and arm posture in a movement. If an arm posture is very close to a movement before or after it, the proposed algorithm is not applicable.

VI. CONCLUSION

Using the proposed muscle-effort-minimization-inspired method, we achieved replicating natural human arm postures. And the replication error in arm swivel angle was 3.73±3.27 degrees (mean±standard deviation) in the validation experiments. To the best of our knowledge, it is the first time that the high-fidelity HAMM and its IK algorithm in position domain are combined to solve the muscle effort minimization problem globally for replicating natural human arm postures given a desired hand pose. With a biologically meaningful kinematic redundancy resolution criterion and minor assumptions, this method has the potential to be applicable across daily manipulation tasks. Being aware of the desired hand pose and joint limits, the proposed method can fill the gap between replicating natural human arm postures and transferring natural human arm postures to an human-like arm-hand robot in manipulation tasks. And it is of significant importance when an accurate human demonstration is expensive or unavailable. Moreover, further developments in understanding the musculoskeletal model of human arms can contribute to a better replication performance and generalization ability for the proposed method.

REFERENCES

[1] A. Billard and D. Kragic, "Trends and challenges in robot manipulation," *Science*, vol. 364, no. 6446, Jun. 2019, Art. no. eaat8414.

[2] C. Lauretti, F. Cordella, and L. Zollo, "A hybrid joint/Cartesian DMP-based approach for obstacle avoidance of anthropomorphic assistive robots," *Int. J. Social Robot.*, vol. 11, no. 5, pp. 783–796, Dec. 2019.

[3] C. H. Xiong, W. R. Chen, B. Y. Sun, M. J. Liu, S. G. Yue, and W. B. Chen, "Design and implementation of an anthropomorphic hand for replicating human grasping functions," *IEEE Trans. Robot.*, vol. 32, no. 3, pp. 652–671, Jun. 2016.

[4] M. Grebenstein *et al.*, "The DLR hand arm system," in *Proc. IEEE Int. Conf. Robot. Autom.*, May 2011, pp. 3175–3182.

[5] T. Lenzi, J. Lipsey, and J. W. Sensinger, "The RIC Arm—A small anthropomorphic transhumeral prosthesis," *IEEE/ASME Trans. Mechatronics*, vol. 21, no. 6, pp. 2660–2671, Dec. 2016.

[6] J. Hermus, J. Lachner, D. Verdi, and N. Hogan, "Exploiting redundancy to facilitate physical interaction," *IEEE Trans. Robot.*, vol. 38, no. 1, pp. 599–615, Feb. 2022.

[7] J. Zhao, B. Xie, and C. Song, "Generating human-like movements for robotic arms," *Mechanism Mach. Theory*, vol. 81, pp. 107–128, Nov. 2014.

[8] M. Li, W. Guo, R. Lin, C. Wu, and L. Han, "An efficient motion generation method for redundant humanoid robot arm based on the intrinsic principles of human arm motion," *Int. J. Humanoid Robot.*, vol. 15, no. 6, Dec. 2018, Art. no. 1850026.

[9] J. Xia, Z. Jiang, H. Zhang, R. Zhu, and H. Tian, "Dual fast marching tree algorithm for human-like motion planning of anthropomorphic arms with task constraints," *IEEE/ASME Trans. Mechatronics*, vol. 26, no. 5, pp. 2803–2813, Oct. 2021.

[10] J. Yang, T. Marler, and S. Rahmatalla, "Multi-objective optimization-based method for kinematic posture prediction: Development and validation," *Robotica*, vol. 29, no. 2, pp. 245–253, Mar. 2011.

[11] Z. Li, D. Milutinovic, and J. Rosen, "Spatial map of synthesized criteria for the redundancy resolution of human arm movements," *IEEE Trans. Neural Syst. Rehabil. Eng.*, vol. 23, no. 6, pp. 1020–1030, Nov. 2015.

[12] H. Kim, L. M. Miller, N. Byl, G. Abrams, and J. Rosen, "Redundancy resolution of the human arm and an upper limb exoskeleton," *IEEE Trans. Biomed. Eng.*, vol. 59, no. 6, pp. 1770–1779, Jun. 2012.

[13] H. Kim and J. Rosen, "Predicting redundancy of a 7 DOF upper limb exoskeleton toward improved transparency between human and robot," *J. Intell. Robotic Syst.*, vol. 80, no. S1, pp. 99–119, Dec. 2015.

[14] Q.-C. Wu, X.-S. Wang, and F.-P. Du, "Analytical inverse kinematic resolution of a redundant exoskeleton for upper-limb rehabilitation," *Int. J. Humanoid Robot.*, vol. 13, no. 3, Sep. 2016, Art. no. 1550042.

[15] A. M. Zanchettin, L. Bascetta, and P. Rocco, "Achieving humanlike motion: Resolving redundancy for anthropomorphic industrial manipulators," *IEEE Robot. Automat. Mag.*, vol. 20, no. 4, pp. 131–138, Dec. 2013.

[16] W. Liu, D. Chen, and J. J. Steil, "Analytical inverse kinematics solver for anthropomorphic 7-DOF redundant manipulators with human-like configuration constraints," *J. Intell. Robot. Syst.*, vol. 86, no. 1, pp. 63–79, 2017.

[17] H. Su, W. Qi, Y. Hu, H. R. Karimi, G. Ferrigno, and E. D. Momi, "An incremental learning framework for human-like redundancy optimization of anthropomorphic manipulators," *IEEE Trans. Ind. Informat.*, vol. 18, no. 3, pp. 1864–1872, Mar. 2022.

[18] K. Yamane, "Kinematic redundancy resolution for humanoid robots by human motion database," *IEEE Robot. Autom. Lett.*, vol. 5, no. 4, pp. 6948–6955, Oct. 2020.

[19] P. K. Artemiadis, P. T. Katsiaris, and K. J. Kyriakopoulos, "A biomimetic approach to inverse kinematics for a redundant robot arm," *Auton. Robots*, vol. 29, nos. 3–4, pp. 293–308, Nov. 2010.

[20] B. A. P. S. Noronha, M. Wessels, A. Q. L. Keemink, A. Bergsma, and H. F. J. M. Koopman, "An upper limb kinematic graphical model for the prediction of anthropomorphic arm trajectories," in *Proc. 7th IEEE Int. Conf. Biomed. Robot. Biomechatronics (Biorob)*, Aug. 2018, pp. 966–971.

[21] W. Chen, C. Xiong, and S. Yue, "On configuration trajectory formation in spatiotemporal profile for reproducing human hand reaching movement," *IEEE Trans. Cybern.*, vol. 46, no. 3, pp. 804–816, Mar. 2016.

[22] K. R. S. Holzbaur, W. M. Murray, and S. L. Delp, "A model of the upper extremity for simulating musculoskeletal surgery and analyzing neuromuscular control," *Ann. Biomed. Eng.*, vol. 33, no. 6, pp. 829–840, Jun. 2005.

[23] M. Mohri, A. Rostamizadeh, and A. Talwalkar, *Foundations of Machine Learning*. Cambridge, MA, USA: MIT Press, 2018.

[24] P. Morel, P. Ulbrich, and A. Gail, "What makes a reach movement effortful? Physical effort discounting supports common minimization principles in decision making and motor control," *PLOS Biol.*, vol. 15, no. 6, Jun. 2017, Art. no. e2001323.

[25] J. Gaveau, S. Grospretre, B. Berret, D. E. Angelaki, and C. Papaxanthis, "A cross-species neural integration of gravity for motor optimization," *Sci. Adv.*, vol. 7, no. 15, Apr. 2021, Art. no. eabf7800.

[26] L. F. C. Figueredo, R. C. Aguiar, L. Chen, S. Chakrabarty, M. R. Dogar, and A. G. Cohn, "Human comfortability: Integrating ergonomics and muscular-informed metrics for manipulability analysis during human–robot collaboration," *IEEE Robot. Autom. Lett.*, vol. 6, no. 2, pp. 351–358, Apr. 2021.

[27] E. Demircan, A. Murai, O. Khatib, and Y. Nakamura, "Muscular effort for the characterization of human postural behaviors," in *Proc. Exp. Robot., 14th Int. Symp. Exp. Robot.*, M. A. Hsieh, O. Khatib, and V. Kumar, Eds. Cham, Switzerland: Springer, 2016, pp. 685–696.

[28] C. Lamperti, A. M. Zanchettin, and P. Rocco, "A redundancy resolution method for an anthropomorphic dual-arm manipulator based on a musculoskeletal criterion," in *Proc. IEEE/RSJ Int. Conf. Intell. Robots Syst. (IROS)*, Sep. 2015, pp. 1846–1851.

[29] E. Demircan, S. Yung, M. Choi, J. Baschshi, B. Nguyen, and J. Rodriguez, "Operational space analysis of human muscular effort in robot assisted reaching tasks," *Robot. Auto. Syst.*, vol. 125, Mar. 2020, Art. no. 103429.

[30] K. R. Saul *et al.*, "Benchmarking of dynamic simulation predictions in two software platforms using an upper limb musculoskeletal model," *Comput. Methods Biomech. Biomed. Eng.*, vol. 18, no. 13, pp. 1445–1458, 2015.

[31] D. C. McFarland, E. M. McCain, M. N. Poppo, and K. R. Saul, "Spatial dependency of glenohumeral joint stability during dynamic unimanual and bimanual pushing and pulling," *J. Biomech. Eng.*, vol. 141, no. 5, May 2019, Art. no. 051006.

[32] M. Millard, T. Uchida, A. Seth, and S. L. Delp, "Flexing computational muscle: Modeling and simulation of musculotendon dynamics," *J. Biomech. Eng.*, vol. 135, no. 2, Feb. 2013, Art. no. 021005.

[33] S. Kalsi-Ryan *et al.*, "Development of reaching, grasping & manipulation indicators to advance the quality of spinal cord injury rehabilitation: SCI-high project," *J. Spinal Cord Med.*, vol. 44, no. 1, pp. S134–S146, 2021.

[34] J. A. Saunders, "Visual feedback control of hand movements," *J. Neurosci.*, vol. 24, no. 13, pp. 3223–3234, Mar. 2004.

[35] C. He *et al.*, "Anthropomorphic reaching movement generating method for human-like upper limb robot," *IEEE Trans. Cybern.*, early access, Oct. 18, 2021, doi: 10.1109/TCYB.2021.3107341.

[36] J.-Z. Guo *et al.*, "Cortex commands the performance of skilled movement," *eLife*, vol. 4, Dec. 2015, Art. no. e10774.

[37] F. C. Anderson and M. G. Pandy, "Static and dynamic optimization solutions for gait are practically equivalent," *J. Biomech.*, vol. 34, no. 2, pp. 153–161, Feb. 2001.

[38] H. Ananthanarayanan and R. Ordóñez, "Real-time inverse kinematics of $(2n^{+1})$ DOF hyper-redundant manipulator arm via a combined numerical and analytical approach," *Mechanism Mach. Theory*, vol. 91, pp. 209–226, Sep. 2015.

[39] M. Shimizu, H. Kakuya, W. K. Yoon, K. Kitagaki, and K. Kosuge, "Analytical inverse kinematic computation for 7-DOF redundant manipulators with joint limits and its application to redundancy resolution," *IEEE Trans. Robot.*, vol. 24, no. 5, pp. 1131–1142, Oct. 2008.

[40] W. Wiedmeyer, P. Altoe, J. Auberle, C. Ledermann, and T. Kroger, "A real-time-capable closed-form multi-objective redundancy resolution scheme for seven-DoF serial manipulators," *IEEE Robot. Autom. Lett.*, vol. 6, no. 2, pp. 431–438, Apr. 2021.

[41] J. Ha, D. Kang, and F. C. Park, "A stochastic global optimization algorithm for the two-frame sensor calibration problem," *IEEE Trans. Ind. Electron.*, vol. 63, no. 4, pp. 2434–2446, Apr. 2016.

[42] A. Seth *et al.*, "OpenSim: Simulating musculoskeletal dynamics and neuromuscular control to study human and animal movement," *PLOS Comput. Biol.*, vol. 14, no. 7, Jul. 2018, Art. no. e1006223.